

Supporting Information.

Hysteresis in the gas sorption isotherms of metal-organic cages accompanied by subtle changes in molecular packing

Gavin A. Craig,^{a†,} Patrick Larpent,^a Hinano Urabe,^a Alexandre Legrand,^a Mickaële Bonneau,^a Shinpei Kusaka,^a and Shuhei Furukawa^{a,b*}*

^aInstitute for Integrated Cell-Material Science (WPI-iCeMS), Kyoto University, Yoshida, Sakyo-ku, Kyoto 606-8501, Japan

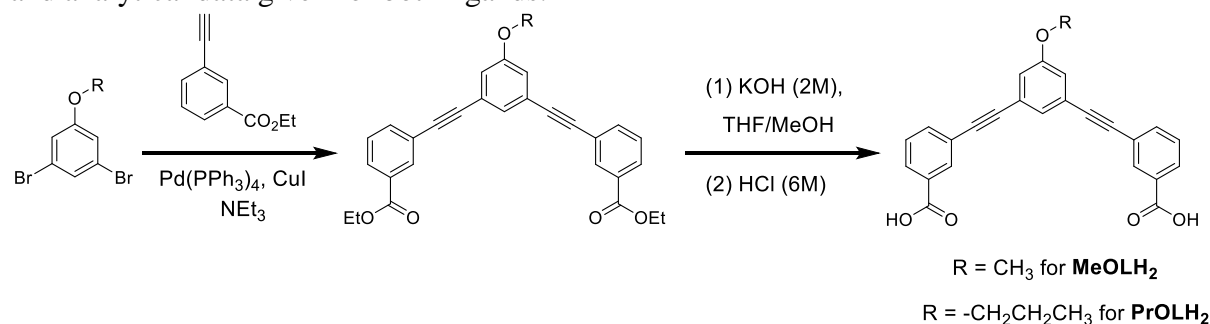
^bDepartment of Synthetic Chemistry and Biological Chemistry, Graduate School of Engineering, Kyoto University, Katsura, Nishikyo-ku, Kyoto 615-8510, Japan.

Table of Contents

Experimental section: synthesis	S3
Experimental section: physical characterization	S5
Table S1. Selected crystallographic data for the structures presented in the main text.	S6
Fig. S1. PLATON analysis of pi-pi interactions in 1	S7
Fig. S2. View of the packing along the <i>a</i> -, <i>b</i> -, and <i>c</i> -axes of 1	S8
Fig. S3. View of the different window sizes in 1	S9
Fig. S4. View of the strain in 2	S9
Fig. S5. PLATON analysis of pi-pi interactions in 2	S10
Fig. S6. View of the packing along the <i>a</i> -, <i>b</i> -, and <i>c</i> -axes of 2	S11
Fig. S7. Comparison of the MeOH phases for MeO-MOC , EtO-MOC , and PrO-MOC	S12
Fig. S8. IR data for MeO-MOC	S12
Fig. S9. IR data for PrO-MOC .	S13
Fig. S10. ¹ H-NMR spectrum of the acid digested bulk sample of 1	S13
Fig. S11. ¹ H-NMR spectrum of the acid digested bulk sample of MeO-MOC after activation	S14
Fig S12. ¹ H-NMR spectrum of the acid digested bulk sample of 2	S14
Fig. S13. ¹ H-NMR spectrum of the acid digested bulk sample of PrO-MOC after activation	S15
Fig. S14. TGA analysis of MeO-MOC	S15
Fig. S15. TGA analysis of PrO-MOC	S16
Fig. S16. N ₂ gas adsorption isotherms for MeO-MOC and PrO-MOC	S16
Fig. S17. CO ₂ gas adsorption isotherms for MeO-MOC and PrO-MOC , and comparison with the rigid phase of EtO-MOC	S17
Fig. S18. Simultaneous gas sorption-PXRD measurements for MeO-MOC	S17
Fig. S19. Comparison of the CO ₂ adsorption isotherms for MeO-MOC and the flexible phase of EtO-MOC	S18
Fig. S20. SEM images of MeO-MOC .	S18

Experimental details.

Synthesis. Solvents and starting reagents were used as purchased from Wako (Japan) or Sigma Aldrich without further purification. The same synthetic route was used for both 3,3'-((5-propoxy-1,3-phenylene)bis(ethyne-2,1-diyl))dibenzoic acid (**PrOLH₂**) and 3,3'-((5-methoxy-1,3-phenylene)bis(ethyne-2,1-diyl))dibenzoic acid (**MeOLH₂**). Ethyl 3-ethynylbenzoate was prepared according to a reported procedure.¹ The detailed procedure is provided for PrOLH₂, and analytical data given for both ligands.



Scheme 1. Synthetic route used to the synthesize the ligands 3,3'-((5-propoxy-1,3-phenylene)bis(ethyne-2,1-diyl))dibenzoic acid (**PrOLH₂**) and 3,3'-((5-methoxy-1,3-phenylene)bis(ethyne-2,1-diyl))dibenzoic acid (**MeOLH₂**).

Diethyl 3,3'-((5-propoxy-1,3-phenylene)bis(ethyne-2,1-diyl))dibenzoate. 1,3-Dibromo-5-propoxybenzene (3.0 g, 10.2 mmol) was dissolved in triethylamine (200 mL) and purged with argon for 15 minutes. Ethyl 3-ethynylbenzoate (3.9 g, 2.2 eq.) was added, followed by Tetrakis(triphenylphosphine)palladium(0) (300 mg) and copper (I) iodide (100 mg). The reaction mixture was stirred at room temperature for 20 minutes, before being heated gradually to 80 °C under argon flow, and then left overnight. The resulting brown suspension cooled to room temperature and filtered over Celite. The filtrate was reduced *in vacuo* to an orange-brown oil, which was purified by column chromatography over silica with hexane:dichloromethane (1:1) as eluent. The combined fractions were reduced to dryness, and the resulting yellow powder recrystallised from a mixture of dichloromethane:methanol (1:6) to yield a white precipitate. Yield, 3.0 g, 61 %. ¹H-NMR (CDCl₃, 500 MHz, 25 °C) δ (ppm): 8.20 (t, 2H, ⁴J = 1.4 Hz), 8.01 (dt, 2H, ³J = 7.9 Hz, ⁴J = 1.4 Hz), 7.69 (dt, 2H, ³J = 7.8 Hz, ⁴J = 1.4 Hz), 7.43 (t, 2H, ³J = 7.8 Hz), 7.33 (s, 1H, ⁴J = 1.1 Hz), 7.06 (d, 2H, ⁴J = 1.4 Hz), 4.40 (q, 4H, ³J = 7.2 Hz), 3.96 (q, 2H, ³J = 6.6 Hz), 1.83 (m, 2H), 1.41 (t, 6H, ³J = 7.2 Hz), 1.05 (t, 3H, ³J = 7.2 Hz).

Diethyl 3,3'-((5-methoxy-1,3-phenylene)bis(ethyne-2,1-diyl))dibenzoate. The same procedure was followed, using 1,3-dibromo-5-methoxybenzene (1.7 g, 6.4 mmol) as starting material. Yield, 2.5 g, 86 %. ¹H-NMR (CDCl₃, 500 MHz, 25 °C) δ (ppm): 8.21 (s, 2H), 8.02 (dt, 2H, ³J = 7.9 Hz, ⁴J = 1.2 Hz), 7.70 (dt, 2H, ³J = 7.7 Hz, ⁴J = 1.2 Hz), 7.44 (t, 2H, ³J = 7.7 Hz), 7.35 (s, 1H), 7.07 (s, 2H), 4.40 (q, 4H, ³J = 7.2 Hz), 3.86 (s, 3H), 1.42 (t, 6H, ³J = 7.2 Hz).

3,3'-((5-propoxy-1,3-phenylene)bis(ethyne-2,1-diyl))dibenzoic acid (PrOLH₂). Diethyl 3,3'-((5-propoxy-1,3-phenylene)bis(ethyne-2,1-diyl))dibenzoate (2.50 g, 5.2 mmol) was dissolved in THF/MeOH (2:1, 60 mL), and 10 mL of 2M aqueous solution of KOH was added. The mixture was stirred at 50°C for three hours. The organic solvents were removed *in vacuo*, and the remaining basic solution was acidified to pH = 1 with HCl (6 M). The resulting white suspension was filtered, and the white precipitate washed with water and then dried under vacuum at 50°C. Yield 2.1 g, 95%. Elemental Analysis (%) Found (Calc.): C 76.17 (76.40), H

4.61 (4.75). $^1\text{H-NMR}$ (DMSO-d_6 , 500 MHz, 25 °C) δ (ppm): 13.25 (br, 2H), 8.10 (s, 2H), 7.98 (d, 2H, $^3\text{J} = 7.8$ Hz), 7.80 (d, 2H, $^3\text{J} = 7.7$ Hz), 7.58 (t, 2H, $^3\text{J} = 7.8$ Hz), 7.38 (s, 1H), 7.21 (s, 2H), 4.01 (t, 2H, $^3\text{J} = 6.4$ Hz), 1.74 (sext, 2H, $^3\text{J} = 6.7$ Hz), 0.98 (t, 2H, $^3\text{J} = 7.3$ Hz). $^{13}\text{C-NMR}$ (DMSO-d_6 , 125 MHz, 25 °C) δ (ppm): 166.9, 159.2, 135.9, 132.6, 131.9, 130.1, 129.7, 127.1, 124.1, 122.9, 118.6, 89.5, 89.3, 69.9, 22.4, 10.7.

3,3'-((5-methoxy-1,3-phenylene)bis(ethyne-2,1-diyl))dibenzoic acid (MeOLH₂). Starting from diethyl 3,3'-((5-methoxy-1,3-phenylene)bis(ethyne-2,1-diyl))dibenzoate (2.50 g, 5.5 mmol) yielded 1.8 g of the title compound. Yield 87%. Elemental Analysis (%) Found (Calc.): C 75.75 (75.59), H 4.07 (4.09). $^1\text{H-NMR}$ (DMSO-d_6 , 500 MHz, 25 °C) δ (ppm): 13.25 (br, 2H), 8.10 (s, 2H), 7.98 (d, 2H, $^3\text{J} = 7.7$ Hz), 7.81 (d, 2H, $^3\text{J} = 7.6$ Hz), 7.58 (t, 2H, $^3\text{J} = 7.7$ Hz), 7.41 (s, 1H), 7.23 (s, 2H), 3.84 (s, 3H). $^{13}\text{C-NMR}$ (DMSO-d_6 , 125 MHz, 25 °C) δ (ppm): 166.9, 159.8, 135.9, 132.6, 131.9, 130.1, 129.8, 127.3, 124.1, 122.8, 118.1, 89.5, 89.4, 56.1.

[Cu₄(MeOL)₄(H₂O)₂(DMA)₂] \cdot 5 DMA \cdot 2 H₂O (1). A solution of MeOLH₂ (70.0 mg, 0.18 mmol) in DMA (2.1 mL) was mixed with a solution of Cu(OAc)₂ \cdot H₂O (35.0 mg, 0.18 mmol) in DMA (2.1 mL), and the green-blue solution left to stir at room temperature. After 1 hour, MeOH (4.2 mL) was quickly added, giving a pale blue suspension. After leaving overnight, the suspension was filtered to give the bulk powder of compound **1**; yield 104 mg. Single crystals suitable for X-ray diffraction were obtained by layering the initial DMA solution with MeOH (1:1 v:v). Blue blocks formed within several hours. The bulk powder was solvent exchanged with MeOH once per day for one week, giving 56 mg of a blue powder (The IR spectra for the crystals, bulk powder, and solvent exchanged powders are shown in Fig. S1. Elemental Analysis after gas sorption measurements (%) Found (Calc.)

[Cu₄(MeOL)₄(H₂O)₄] \cdot (H₂O) (%) Found (Calc.): C 62.48 (62.50), H 3.26 (3.46).

[Cu₄(PrOL)₄(MeOH)₂(DMF)₂] 5 DMF (2). PrOLH₂ (117 mg, 0.28 mmol) in DMF (2.0 mL) was mixed with Cu(OAc)₂ \cdot H₂O (50 mg, 0.25 mmol) in DMF (2.0 mL) to give a blue solution. This solution was left to stand for one hour at room temperature before 4 mL of MeOH were added causing the solution to become turbid. After 24 hours, the blue suspension contained some off-white powder from unreacted ligand and 124 mg of a blue crystalline powder, which could be separated by decantation. The blue crystals were washed with MeOH/DMF (1/1) and left to dry in air. Single crystals were prepared by mixing a solution of PrOLH₂ (11.7 mg, 0.028 mmol) in DMF (0.5 mL) was mixed with a solution of Cu(OAc)₂ \cdot H₂O (5 mg, 0.025 mmol) in DMF (0.5 mL), before layering the resulting solution with 1 mL of MeOH. Blue plate crystals suitable for X-ray diffraction formed within one day. (The IR spectra for the crystals, bulk powder, and solvent exchanged powders are shown in Fig. S2). Elemental Analysis (%) Found (Calc.) for [Cu₄(PrOL)₄(H₂O)₄] \cdot (H₂O) (%): C 64.08 (63.78), H 4.09 (4.06).

Physical characterization

^1H and ^{13}C NMR spectra were measured with a Bruker Ultrashield 500 plus (500 MHz) spectrometer at 25°C. For acid digestion of the complexes, *ca.* 15 mg of the complex were suspended in DMSO-*d*₆ and 40 μL of DCL solution were added, and the mixture was left to stand for 5 hours at RT. The resulting solution was used directly for NMR spectroscopy. Infrared spectra were collected on neat samples using a Jasco FT/IR-6100 spectrometer. Thermogravimetric analyses (TGA) were performed with a Rigaku model Thermo plus EVO

under N₂ using a heating rate of 5 °C min⁻¹. Powder X-ray diffraction data were collected using a Rigaku SmartLab diffractometer equipped with Cu K α radiation ($\lambda = 1.54056 \text{ \AA}$). The samples for gas sorption were activated in situ by heating under vacuum to 120 °C for 16 hours, before measurement of the isotherms at 77 K (N₂) and 195 K (CO₂) using a BELSORP-max volumetric adsorption instrument from BEL Japan, Inc.. The temperature of the samples was controlled using a cryostat. In situ gas adsorption–PXRD measurements for **MeO-MOC** were performed on a Rigaku SmartLab diffractometer with Cu K α radiation connected to a BELSORP-18PLUS volumetric adsorption instrument (BEL Japan, Inc.). The instruments were automated and synchronised with each other, and an X-ray diffraction pattern was obtained at each equilibrium point in the adsorption isotherm. Scanning electron microscopy images of **MeO-MOC** were collected using a JEOL Model JSM-7001F4 system.

Single crystal XRD

Crystallographic intensity data were collected using a Rigaku model XtaLAB P200 diffractometer equipped with a Dectris model PILATUS 200K detector and confocal monochromated Mo K α radiation ($\lambda = 0.71075 \text{ \AA}$). All structures were solved with the ShelXT structure solution program² using intrinsic phasing, and refined with ShelXL³ using least squares minimisation (Table S1), within the program Olex 2.1.⁴ For both compounds, the SQUEEZE algorithm in PLATON was used to account for areas of diffuse solvent.⁵

In compound **1**, all non-hydrogen atoms on the skeleton of the main MOC molecule were refined anisotropically, with the exception of the C atom of the MeOH that is coordinated to the inner axial site of the copper paddlewheel. This MeOH molecule has a partial occupancy of 0.25, with a water molecule occupying the site for the remaining 0.75. The external paddlewheel site is occupied by a DMA molecule split over two positions in a 0.27:0.73 ratio. Two partially occupied DMA molecules were included in the model with occupancies fixed at 0.2 and 0.5. SQUEEZE was used to account for the remaining electron density, calculating a solvent accessible volume of 1485 Å³ per unit cell containing 378 electrons (or 189 electrons per MOC). This can be approximately accounted for by four DMA molecules (192 electrons).

In compound **2**, all non-hydrogen atoms were refined anisotropically. Hydrogen atoms were placed in calculated positions and refined with a riding model. The contribution from disordered solvent was accounted for using SQUEEZE, which gave a solvent accessible volume of 2043 Å³ per unit cell containing 480 electrons (or 240 electrons per MOC molecule). This can be accounted for approximately by six DMF molecules per molecule of MOC (240 electrons).

The .cif files for these structures have been submitted to the Cambridge Structural Database: CSD Numbers 1966329 (**1**) and 1966328 (**2**). These data can be obtained free of charge from The Cambridge Crystallographic Data Centre via www.ccdc.cam.ac.uk/data_request/cif.

Table S1. Selected crystallographic data for the crystal structures presented in the main text.

	1	2
λ (Å)	0.71073	
T (K)	100	
Crystal System	Monoclinic	Monoclinic
Space Group	$P2_1/n$	$P2/n$
a (Å)	14.2345(3)	15.2966(4)
b (Å)	29.3603(5)	17.7385(3)
c (Å)	16.5980(4)	24.6648(5)
α (°)	90	90
β (°)	111.254(3)	95.051(2)
γ (°)	90	90
V (Å ³)	6465.0(3)	6666.5(2)
Z	2	2
D_{calc} (g cm ⁻³)	1.276	1.292
Reflections	78435	84020
Unique Data	12704	12664
R_{int}	0.037	0.044
$R[F^2 > 2\sigma(F^2)]$	0.060	0.054
$wR(F^2)$	0.175	0.169
S	1.07	1.04
$\rho_{\text{max}}, \rho_{\text{min}}$ (eÅ ⁻³)	0.98, -0.60	0.88, -0.56

```

=====
Analysis of Short Ring-Interactions with Cg-Cg Distances < 6.0 Ang., Alpha < 20.000 Deg. and Beta < 60.0 Deg.
=====
- Cg(I) = Plane number I (= ring number in () above)
- Alpha = Dihedral Angle between Planes I and J (Deg)
- Beta = Angle Cg(I)-->Cg(J) or Cg(I)-->Me vector and normal to plane I (Deg)
- Gamma = Angle Cg(I)-->Cg(J) vector and normal to plane J (Deg)
- Cg-Cg = Distance between ring Centroids (Ang.)
- CgI_Perp = Perpendicular distance of Cg(I) on ring J (Ang.)
- CgJ_Perp = Perpendicular distance of Cg(J) on ring I (Ang.)
- Slippage = Distance between Cg(I) and Perpendicular Projection of Cg(J) on Ring I (Ang.)
- P,Q,R,S = J-Plane Parameters for Carth. Coord. (Xo, Yo, Zo)

Cg(I) Res(I) Cg(J) [ ARU(J)] Cg-Cg Transformed J-Plane P, Q, R, S Alpha Beta Gamma CgI_Perp CgJ_Perp Slippage
Cg1 [ 1] -> Cg2 [ 4565.01] 3.6228(19) 0.9692-0.2427-0.0413 -5.7163 2.65(16) 21.3 20.4 3.3954(13) 3.3764(15) 1.313
Cg1 [ 1] -> Cg6 [ 4465.01] 5.439(2) -0.2849-0.8204 0.4957 -12.3136 81.86(17) 27.9 71.5 1.7261(13) 4.8089(17)
Cg2 [ 1] -> Cg1 [ 4464.01] 3.6228(19) 0.9747 0.2108-0.0744 -3.0020 2.65(16) 20.4 21.3 3.3764(15) 3.3954(13) 1.263
Cg3 [ 1] -> Cg3 [ 3567.01] 3.8704(19) -0.9373-0.0602-0.3433 1.1275 0.00(16) 29.6 29.6 3.3641(14) 3.3640(14) 1.914
Cg3 [ 1] -> Cg5 [ 3667.01] 5.189(2) 0.2038-0.7251-0.6578 -24.1808 85.50(17) 16.1 69.6 1.8128(13) 4.9852(17)
Cg5 [ 1] -> Cg1 [ 2546.01] 5.8226(19) -0.9747-0.2108 0.0744 -2.1768 84.57(16) 25.1 74.2 1.5815(17) 5.2729(13)
Cg5 [ 1] -> Cg6 [ 3666.01] 4.620(2) 0.2849-0.8204-0.4957 -12.3162 11.76(18) 46.0 38.9 3.5938(15) 3.2093(16) 3.323
Cg6 [ 1] -> Cg3 [ 1554.01] 5.273(2) 0.9373 0.0602 0.3433 2.5661 87.28(17) 24.5 68.5 1.9324(17) 4.7959(13)
Cg6 [ 1] -> Cg5 [ 3666.01] 4.620(2) 0.2038-0.7251-0.6578 -12.7785 11.76(18) 38.9 46.0 3.2093(16) 3.5938(15) 2.903

Min or Max 3.623 0.0 16.1 74.2 -3.594 -5.273

[ 4565] = 1/2+X,3/2-Y,1/2+Z
[ 4465] = -1/2+X,3/2-Y,1/2+Z
[ 4464] = -1/2+X,3/2-Y,-1/2+Z
[ 3567] = -X,1-Y,2-Z
[ 3667] = 1-X,1-Y,2-Z
[ 2546] = 1/2-X,-1/2+Y,3/2-Z
[ 3666] = 1-X,1-Y,1-Z
[ 1554] = X,Y,-1+Z

```

"gac354_sq" PLATON-GEOMETRY Page 88

```

=====
Analysis of X-H...Cg(Pi-Ring) Interactions (H..Cg < 3.0 Ang. - Gamma < 40.0 Deg)
=====
- Cg(J) = Center of gravity of ring J (Plane number above)
- H-Perp = Perpendicular distance of H to ring plane J
- Gamma = Angle between Cg-H vector and ring J normal
- X-H..Cg = X-H-Cg angle (degrees)
- X..Cg = Distance of X to Cg (Angstrom)
- X-H, Pi = Angle of the X-H bond with the Pi-plane (i.e.' Perpendicular = 90 degrees, Parallel = 0 degrees)

X--H(I) Res(I) Cg(J) [ ARU(J)] H..Cg Transformed J-Plane P, Q, R, S H-Perp Gamma X-H..Cg X..Cg X-H,Pi
C35 -H35A [ 2] -> Cg4 [ 1555.01] 2.91 0.6948-0.5846-0.4191 -10.6364 2.80 15.74 135 3.661(11) 61
C74 -H74B [ 1] -> Cg6 [ 4464.01] 2.99 -0.2849-0.8204 0.4957 -21.6964 2.86 16.49 115 3.507(12) 36
C75 -H75C [ 1] -> Cg2 [ 4464.01] 2.91 0.9692-0.2427-0.0413 -13.0426 2.90 3.82 123 3.517(14) 31
C81 -H81B [ 1] -> Cg2 [ 4464.01] 2.94 0.9692-0.2427-0.0413 -13.0426 2.52 30.93 158 3.84(2) 44
C84 -H84A [ 1] -> Cg6 [ 4464.01] 2.70 -0.2849-0.8204 0.4957 -21.6964 2.34 29.96 170 3.65(3) 67

Min or Max 2.700 2.343 3.8 170.00 3.507 67.00

```

Fig. S1. PLATON analysis of the π - π interactions found in **1**.

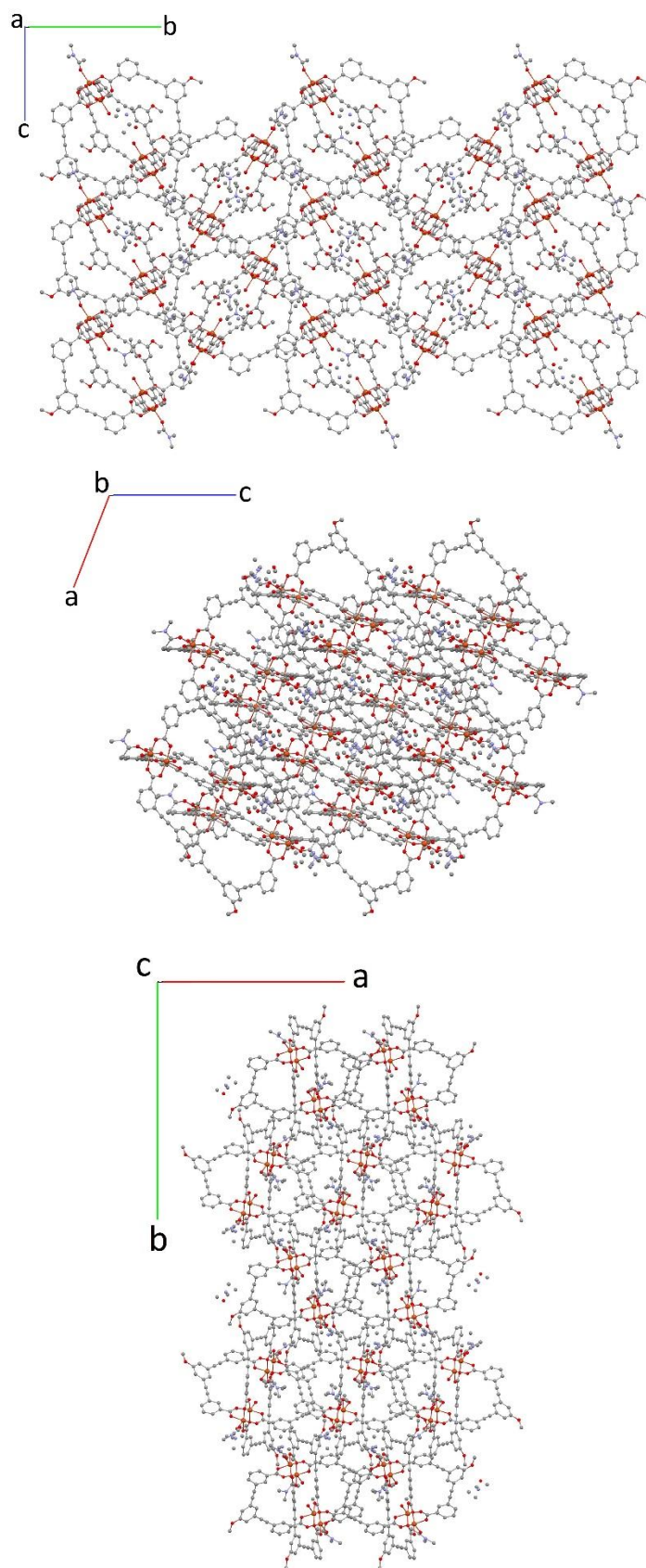


Figure S2. View along the *a*- (top), *b*- (middle), and *c*-axes (bottom) of **1**, illustrating that the overall arrangement of the molecules does not lead to any discernible channels in the crystal structure.

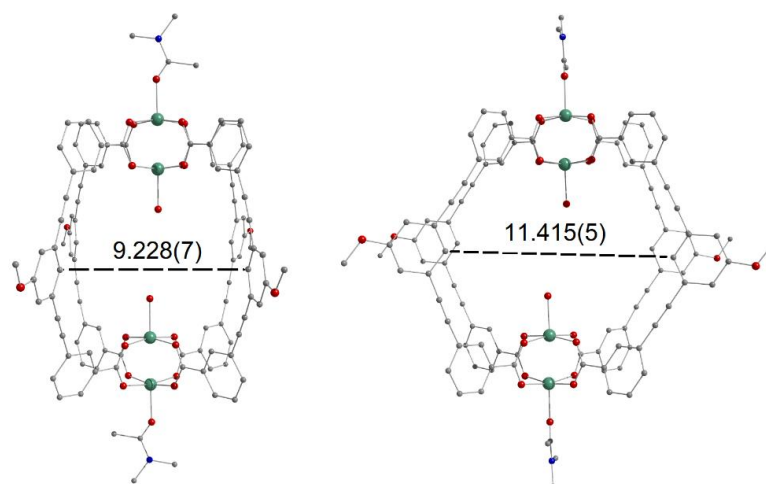


Figure S3. The dibenzoate ligands in **1** are puckered, leading to two different window sizes in the MOC molecule in the crystal structure, one measuring 9.228(7) Å from C4 to C29 and another measuring 11.415(5) Å from C4 to C29'.

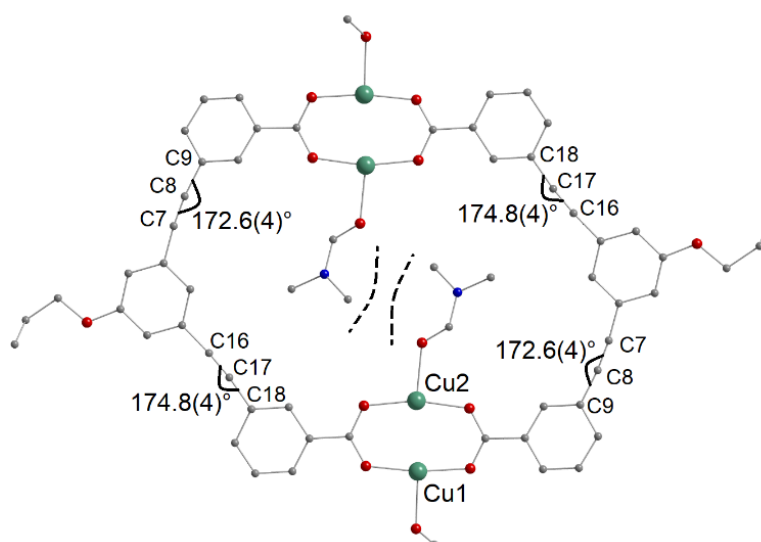


Figure S4. Illustration of the strain induced in **Pro-MOC** caused by the coordination of the DMF molecules inside the cage rather than outside. For clarity, two of the dibenzoate ligands have been omitted, as well as hydrogen atoms.

↑

Analysis of Short Ring-Interactions with Cg-Cg Distances < 6.0 Ang., Alpha < 20.000 Deg. and Beta < 60.0 Deg.

-
- Cg(I) = Plane number I (= ring number in () above)
 - Alpha = Dihedral Angle between Planes I and J (Deg)
 - Beta = Angle Cg(I)-->Cg(J) or Cg(I)-->Me vector and normal to plane I (Deg)
 - Gamma = Angle Cg(I)-->Cg(J) vector and normal to plane J (Deg)
 - Cg-Cg = Distance between ring Centroids (Ang.)
 - CgI_Perp = Perpendicular distance of Cg(I) on ring J (Ang.)
 - CgJ_Perp = Perpendicular distance of Cg(J) on ring I (Ang.)
 - Slippage = Distance between Cg(I) and Perpendicular Projection of Cg(J) on Ring I (Ang.)
 - P,Q,R,S = J-Plane Parameters for Carth. Coord. (Xo, Yo, Zo)

Cg(I)	Res(I)	Cg(J)	[ARU(J)]	Cg-Cg	Transformed	J-Plane P, Q, R, S	Alpha	Beta	Gamma	CgI_Perp	CgJ_Perp	Slippage
Cg1	[1] -> Cg1	[3666.01]		4.939(2)	-0.1309-0.5737-0.8085	-17.6739	0.03(17)	43.4	43.4	3.5882(15)	3.5883(15)	3.393
Cg1	[1] -> Cg3	[3666.01]		4.942(2)	-0.2385-0.5550-0.7969	-18.1176	6.30(18)	46.8	45.0	3.4922(15)	3.3827(16)	3.603
Cg1	[1] -> Cg4	[2555.01]		5.557(2)	-0.9993 0.0349 0.0140	-8.9669	84.3(2)	26.3	69.5	1.9477(17)	-4.9821(14)	
Cg2	[1] -> Cg3	[3666.01]		5.819(2)	-0.2385-0.5550-0.7969	-18.1176	20.11(18)	57.8	55.8	3.2718(15)	3.1025(16)	
Cg2	[1] -> Cg5	[4565.01]		4.7670(19)	0.8658 0.0308-0.4995	-5.2143	78.02(17)	16.8	80.1	0.8165(16)	4.5636(14)	
Cg2	[1] -> Cg6	[3556.01]		5.504(2)	-0.9733 0.2212 0.0616	0.1234	82.16(17)	32.8	65.5	-2.2800(16)	-4.6261(13)	
Cg3	[1] -> Cg1	[3666.01]		4.942(2)	-0.1309-0.5737-0.8085	-17.6739	6.30(18)	45.0	46.8	3.3828(16)	3.4922(15)	3.497
Cg3	[1] -> Cg2	[3666.01]		5.819(2)	-0.0785-0.7956-0.6008	-18.0728	20.11(18)	55.8	57.8	3.1026(16)	3.2718(15)	
Cg3	[1] -> Cg3	[2555.01]		5.095(2)	-0.2385 0.5550-0.7969	3.0824	67.43(18)	34.6	34.6	-4.1937(15)	-4.1938(15)	
Cg4	[1] -> Cg4	[2455.01]		3.955(3)	-0.9993 0.0349 0.0140	6.3189	4.0(2)	28.5	28.5	-3.4761(19)	-3.4760(19)	1.887
Cg5	[1] -> Cg3	[2555.01]		5.387(2)	-0.2385 0.5550-0.7969	3.0824	79.95(17)	23.7	84.2	-0.5459(14)	4.9326(15)	
Cg5	[1] -> Cg5	[2455.01]		3.760(2)	-0.8658-0.0308 0.4995	8.3917	3.53(16)	6.3	6.3	-3.7369(14)	-3.7369(14)	0.412
Cg6	[1] -> Cg6	[3556.01]		4.059(2)	-0.9733 0.2212 0.0616	0.1234	0.00(17)	33.7	33.7	3.3790(15)	3.3790(15)	2.249
				Min or Max	3.760		0.0	6.3	84.2	-4.194	-4.982	

- [3666] = 1-X,1-Y,1-Z
- [2555] = 1/2-X,Y,1/2-Z
- [4565] = 1/2+X,1-Y,1/2+Z
- [3556] = -X,-Y,1-Z
- [2455] = -1/2-X,Y,1/2-Z

↑

Analysis of X-H...Cg(Pi-Ring) Interactions (H..Cg < 3.0 Ang. - Gamma < 30.0 Deg)

-
- Cg(J) = Center of gravity of ring J (Plane number above)
 - H-Perp = Perpendicular distance of H to ring plane J
 - Gamma = Angle between Cg-H vector and ring J normal
 - X-H..Cg = X-H-Cg angle (degrees)
 - X..Cg = Distance of X to Cg (Angstrom)
 - X-H, Pi = Angle of the X-H bond with the Pi-plane (i.e.' Perpendicular = 90 degrees, Parallel = 0 degrees)

X--H(I)	Res(I)	Cg(J)	[ARU(J)]	H..Cg	Transformed	J-Plane P, Q, R, S	H-Perp	Gamma	X-H..Cg	X..Cg	X-H,Pi
C39	-H39	[1] -> Cg2	[4464.01]	2.64	0.0785-0.7956 0.6008	-10.1774	2.63	5.60	147	3.473(4)	56
				Min or Max	2.640		2.626	5.6	147.00	3.473	56.00

Fig S5. PLATON analysis of the π - π interactions found in 2.

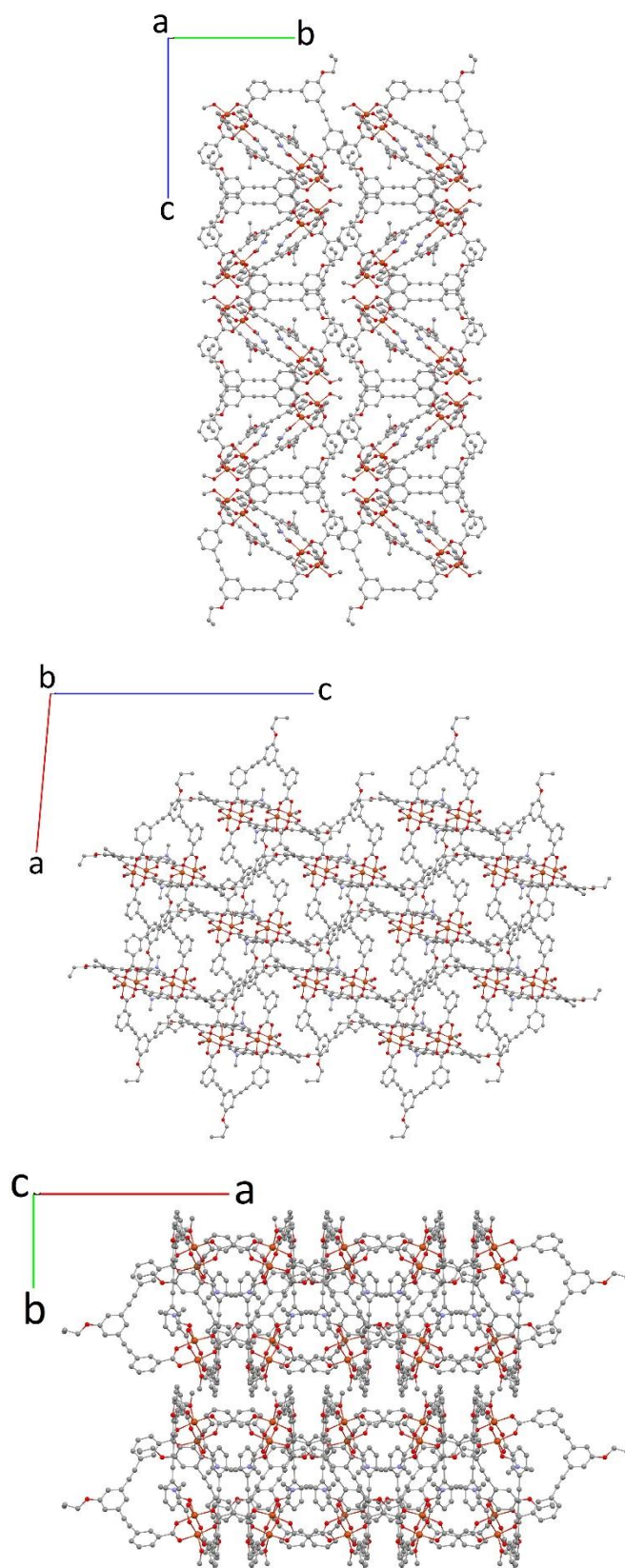


Figure S6. View along the *a*- (top), *b*- (middle), and *c*-axes (bottom) of **2**, illustrating that the overall arrangement of the molecules does not lead to any discernible channels in the crystal structure.

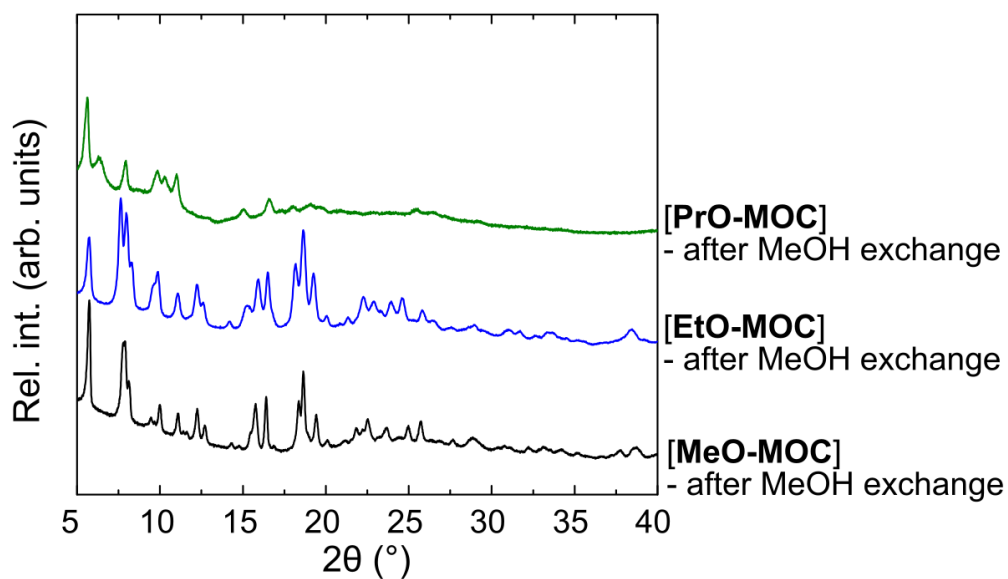


Figure S7. Comparison of the powder X-ray diffraction (PXRD) data collected for all three MOCs subsequent to MeOH exchange.

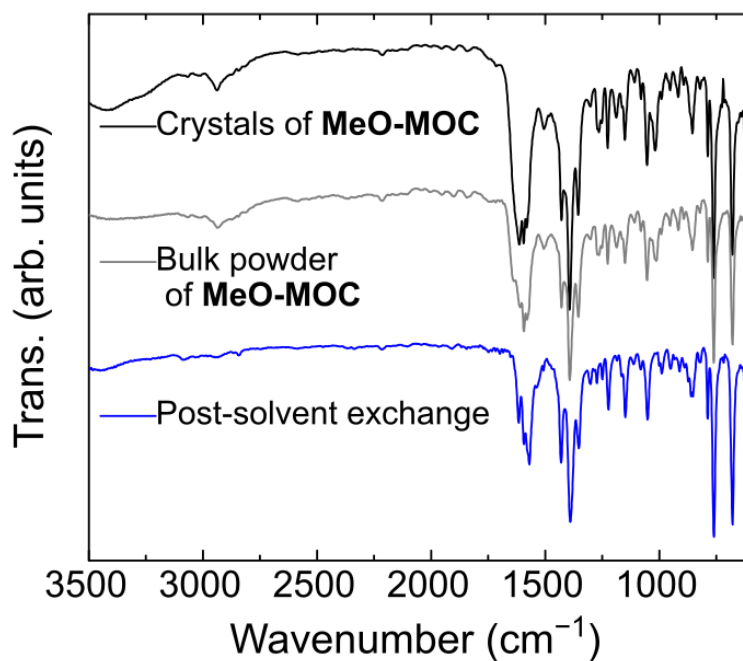


Figure S8. Infra-red (IR) spectra for the various phases of **MeO-MOC**: crystals of compound **1**, the bulk synthesis of compound **1**, and the crystalline powder obtained subsequent to solvent exchange with methanol.

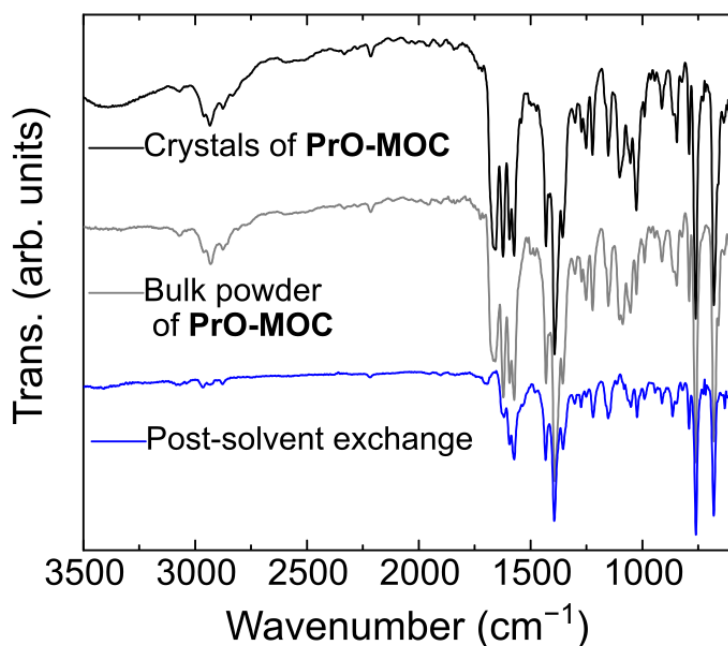


Figure S9. Infra-red (IR) spectra for the various phases of **PrO-MOC**: crystals of compound **2**, the bulk synthesis of compound **2**, and the crystalline powder obtained subsequent to solvent exchange with methanol.

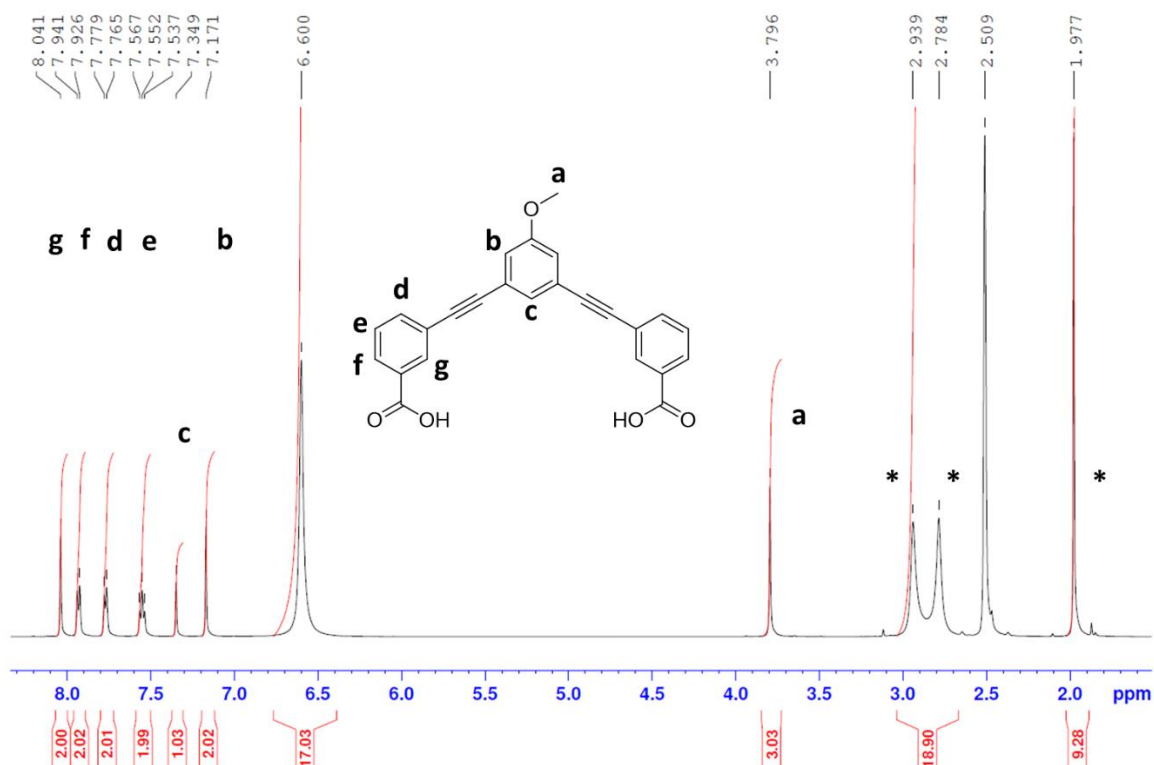


Figure S10. ^1H NMR spectrum of the as synthesised bulk sample of **1** subsequent to digestion in DCI/DMSO. The peaks arising from DMA in the lattice are highlighted with asterisks.

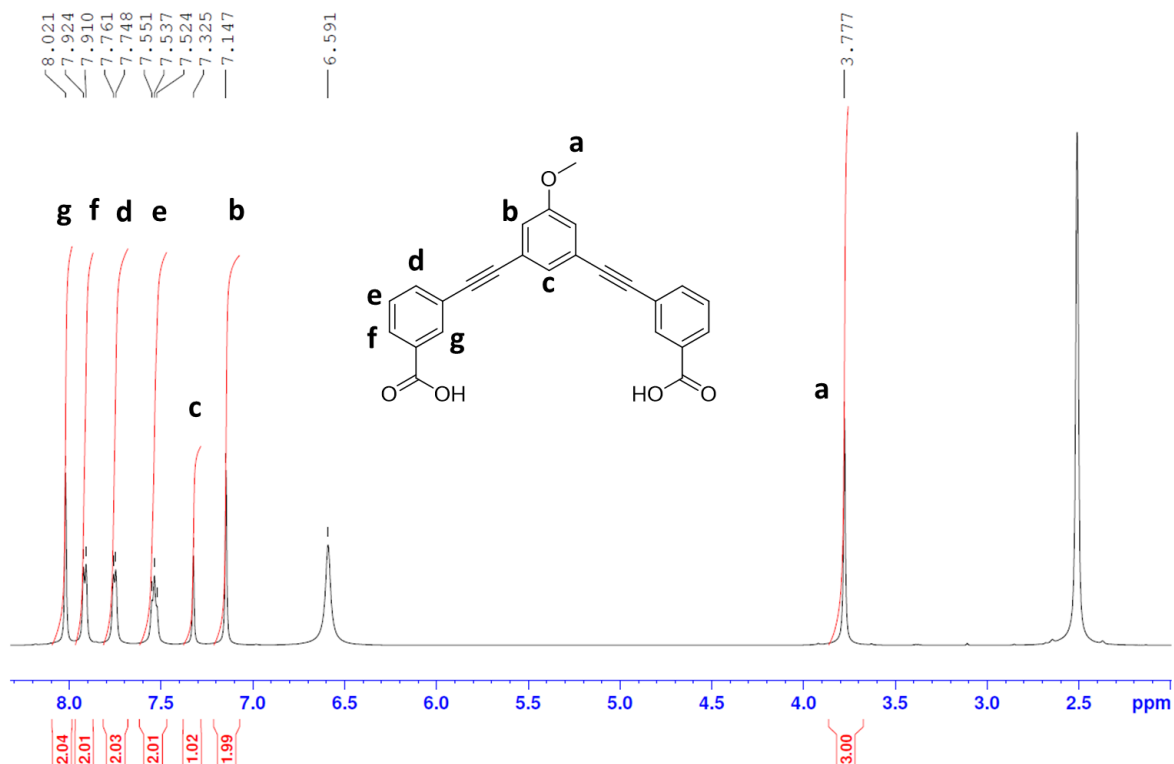


Figure S11. ^1H NMR spectrum of the activated phase **MeO-MOC** subsequent to digestion in DCI/DMSO. The peak for CH_3OH arising from residual MeOH would be expected at 3.14 ppm.

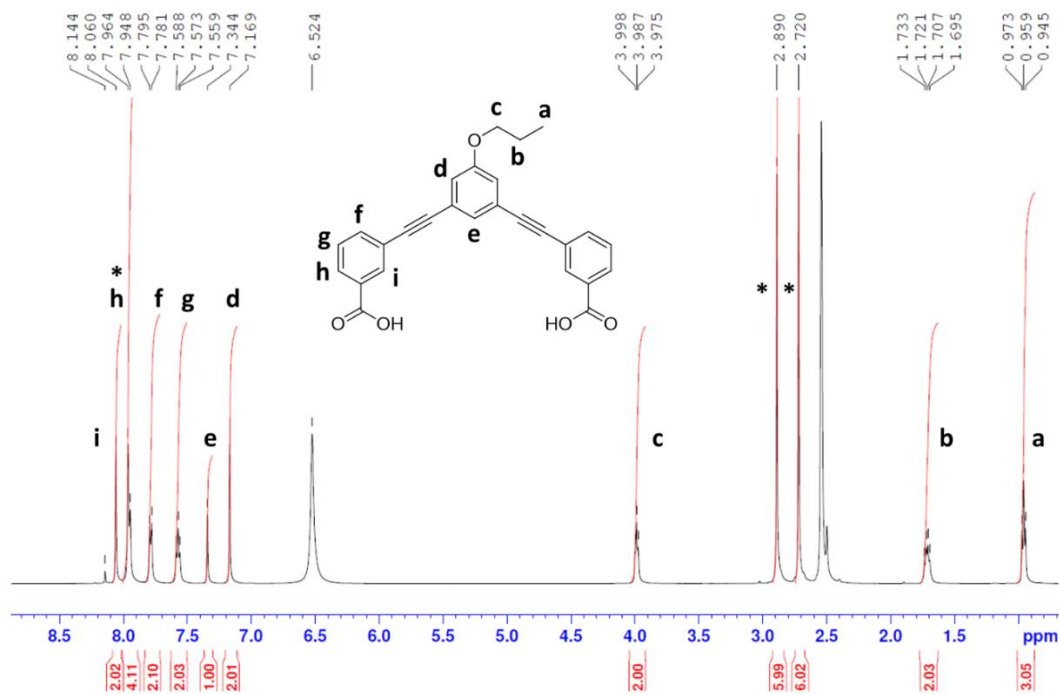


Figure S12. ^1H NMR spectrum of the as synthesised bulk sample of **2** subsequent to digestion in DCI/DMSO. The peaks arising from DMF in the lattice are highlighted with asterisks. The aldehyde proton in DMF overlaps with the signal for proton labelled “h” in the ligand, leading to a higher value for the integral.

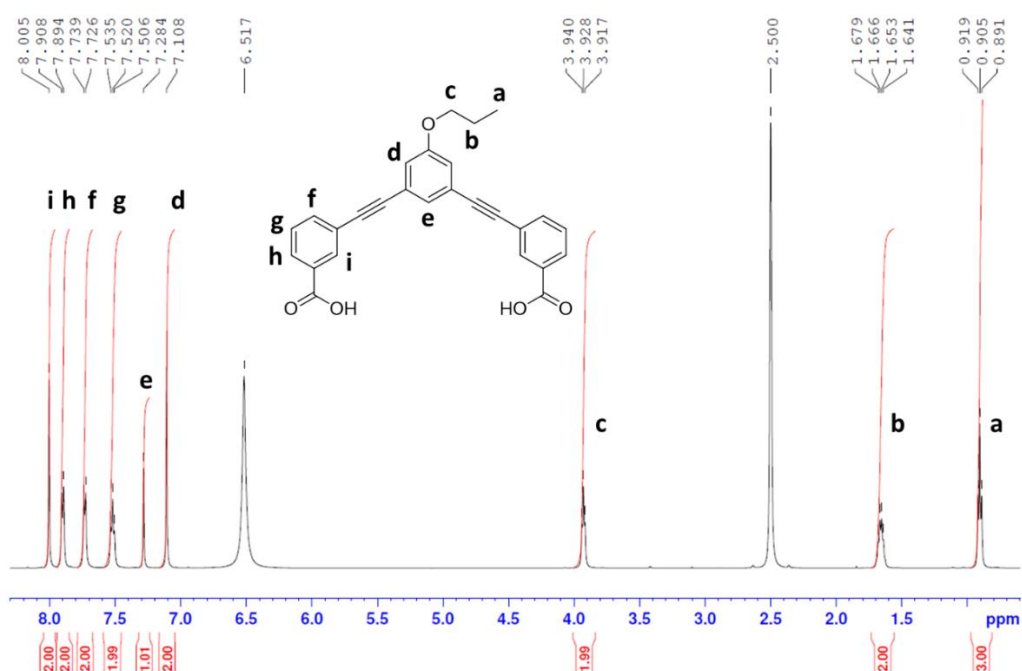


Figure S13. ¹H NMR spectrum of the activated phase **Pro-MOC** subsequent to digestion in DCI/DMSO. The peak for CH_3OH arising from residual MeOH would be expected at 3.14 ppm.

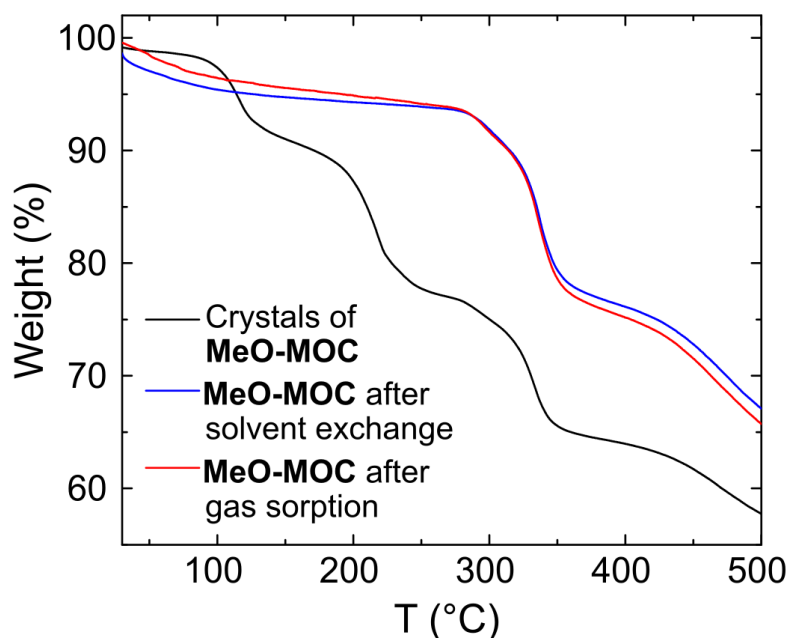


Figure S14. Thermogravimetric analyses recorded for compound **1** and **MeO-MOC** over the temperature range 25 to 500 °C. After solvent exchange and gas sorption, the plateau prior to decomposition at 280 °C corresponds to a weight loss of 6%, which is greater than that expected for loss of only the H_2O molecules bound to the paddlewheels (3.8%), suggesting loss of water molecules absorbed from the atmosphere.

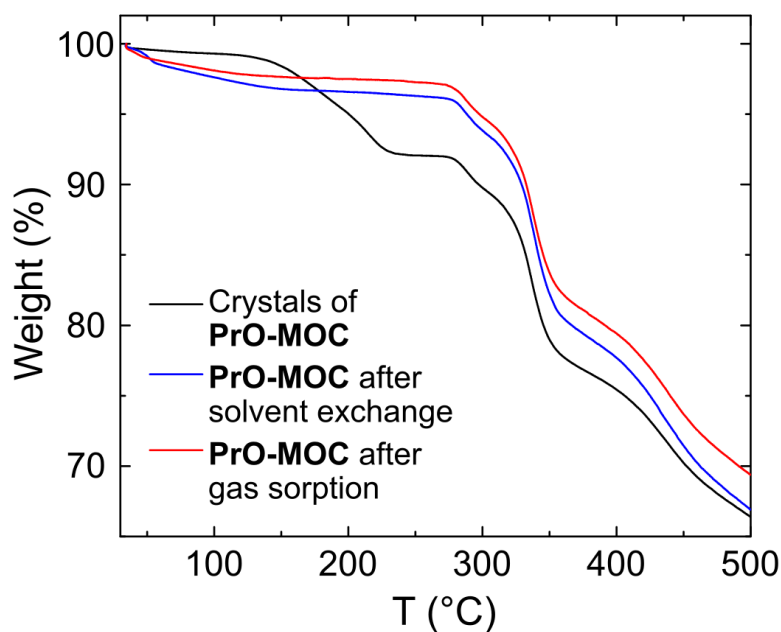


Figure S15. Thermogravimetric analyses recorded for compound **2** and **PrO-MOC** over the temperature range 25 to 500 °C. After solvent exchange and gas sorption, the plateau prior to decomposition at 280 °C corresponds to a weight loss of 4.2% and 3.4 %, respectively, compared to a calculated loss of 3.6% for loss of only H₂O molecules bound to the paddlewheels. After solvent exchange, this suggests loss of further H₂O molecules or MeOH molecules from the sample.

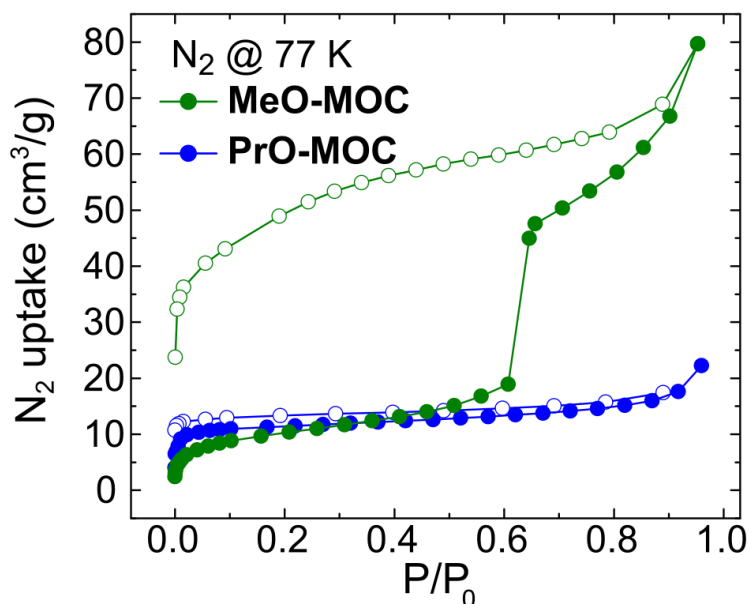


Figure S16. N₂ gas sorption isotherms for **MeO-MOC** and **PrO-MOC**, measured at 77 K. Filled symbols represent adsorption, while empty symbols represent desorption.

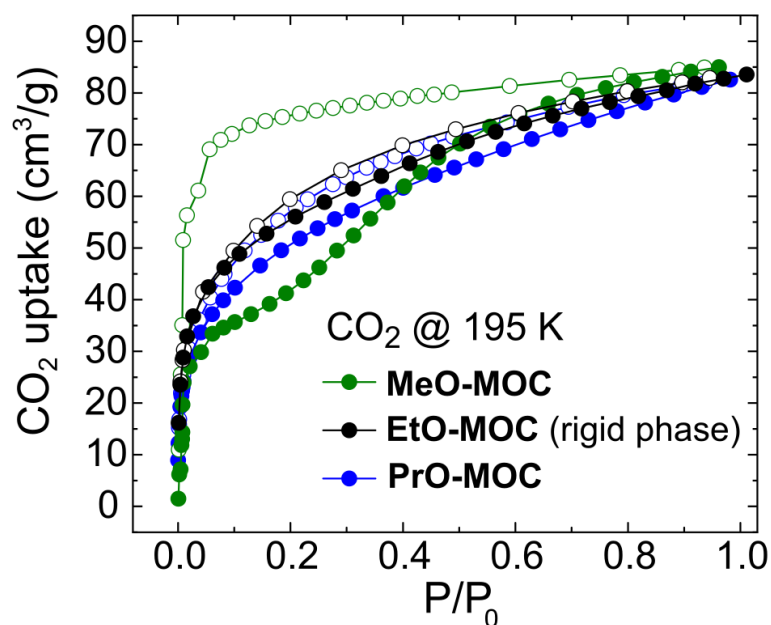


Figure S17. CO₂ gas sorption isotherms for **MeO-MOC** and **PrO-MOC**, measured at 195 K. For comparison, the sorption isotherm for the rigid phase of EtO-MOC is also included. Filled symbols represent adsorption, while empty symbols represent desorption. These phases of the respective cages show similar uptake of CO₂ at 195 K and $P/P_0=1$, suggesting that the overall uptake is determined by the pore of the MOC molecules, which is identical in each case.

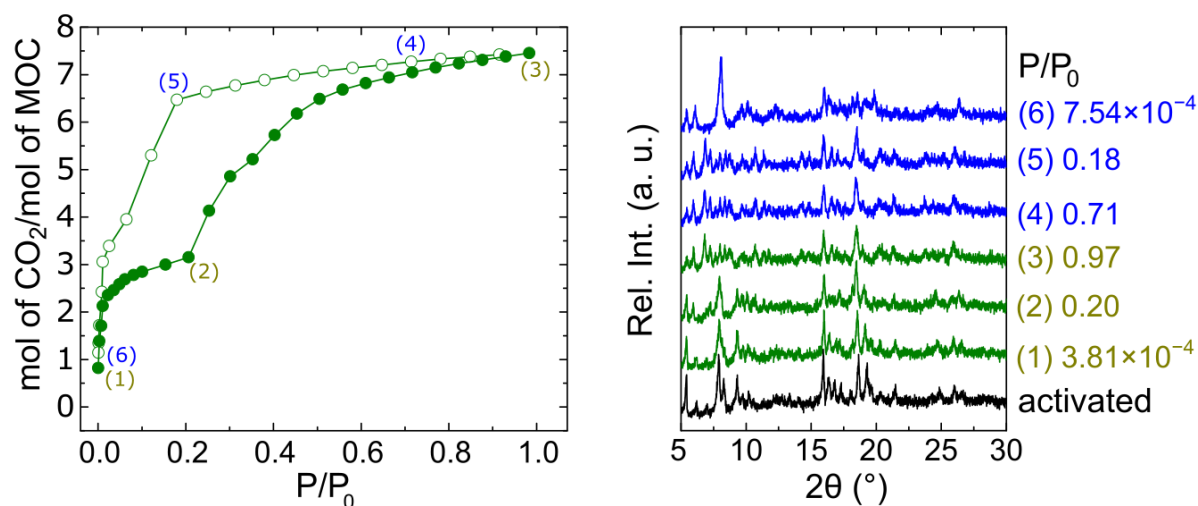


Figure S18. In situ PXRD and gas sorption measurements. (left) CO₂ sorption isotherm measured for **MeO-MOC** at 195 K. The numbers in parenthesis correspond to the powder X-ray diffractograms. (right) Selected PXRD data for **MeO-MOC** collected at the partial pressures shown. The activated phase is shown in black, adsorption measurements are shown in green, and the desorption measurements are shown in blue.

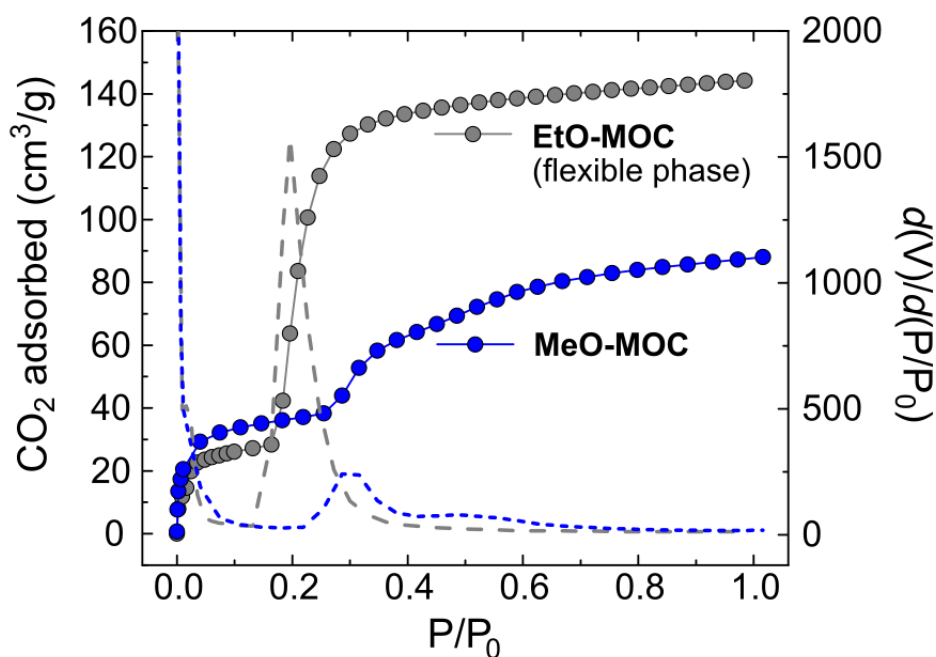


Figure S19. Comparison of the adsorption isotherms of CO₂ measured at 195 K for **MeO-MOC** and the flexible phase of **EtO-MOC**. The dashed lines show the derivative of the isotherms for each compound.

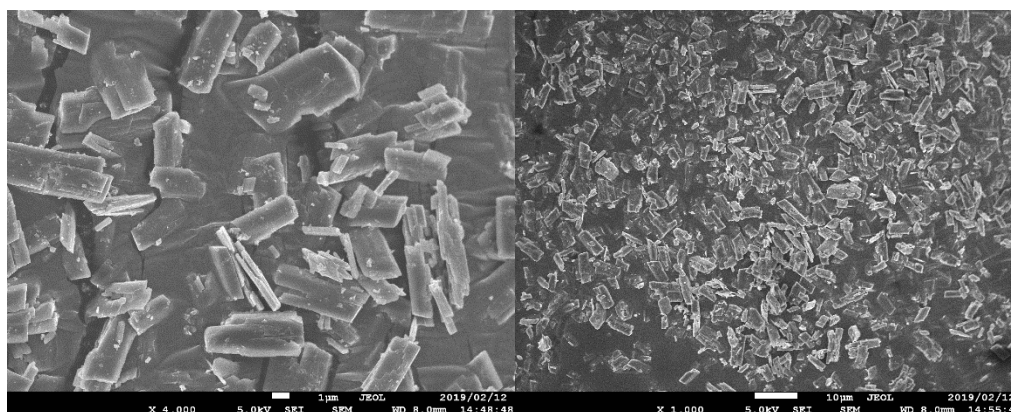


Figure S20. Scanning electron microscopy (SEM) images of the crystallites in **MeO-MOC**. The scale bars measure 1 µm (left) and 10 µm (right).

References

1. J.-R. Li and H.-C. Zhou, *Nature Chem.*, 2010, **2**, 893.
2. G. Sheldrick, *Acta Cryst.*, 2008, **A64**, 112-122.
3. G. Sheldrick, *Acta Cryst.*, 2015, **C71**, 3-8.
4. O. V. Dolomanov, L. J. Bourhis, R. J. Gildea, J. A. K. Howard and H. Puschmann, *J. Appl. Crystallogr.*, 2009, **42**, 339-341.
5. A. L. Spek, *Acta Cryst.*, 2009, **D65**, 148-155.